

Index

Page numbers in *italic* denote figures. Page numbers in **bold** denote tables.

- 3D printing 32–33
- acid fracturing 13
- acid stimulation 10
- acoustic velocity
and porosity, Malta outcrop studies 262–278
see also seismic velocity
- acoustic wavefront imaging 376, 377
- advection-dispersion-reaction equation 24, 27, 40, 212, 213
- aggregate attributes 342–343
- aggregate edge cube 336, 342–343
- aggregate fault cube 17, 335, 336, 343, 344, 347
- algae
calcareous, Shu'aiba Formation 407, 408
coralline, Lower Coralline Limestone 264–265
- Amellago, Morocco, LiDAR images 8
- Amphistegina* 265, 267
- Anadarko Basin 180, 181
- anhydrite
Indian Basin Field 145, 149, 151, 153, 155, 165
- Ant Colony Optimization algorithm 35, 458, 459
- Ant-Tracking edge-enhancement process 342, 345
- aragonite 122
- Archie classification 232
- Arkoma Basin 180, 181
hydrothermal fluid migration 197, 199–200, 202
- Arne-Elin Graben 332, 334
- artificial intelligence 5, 35–36
- asperity 361, 362
see also roughness
- atom-probe tomography 14
- atomic force microscopy (AFM) 4, 11
calcite dissolution 82
- Attard Member 264–265, 266
- Austin Chalk
acoustic wavefront imaging 376, 377
wave guiding 376
- backstripping, diagenetic 4, 11
- Balder unconformity 334, 344, 348, 350
- Basin and Range tectonism 144, 163, 165, 166, 171, 172
- Benicassim, NE Spain, dolomitization 31
- Bentheimer Sandstone
network modelling 98, **100**, 101, 102, 103, 104
cementation study 103, 104–106, 111
stress-dependent velocity anisotropy 363–367
- bioclasts
Lower Coralline Limestone 265
Osagean **184–185**, 186, 187, 203
- Black Oil model 24
- Bourbon Arch 180, 181
- breccia
chert **185**, 186, 188
Indian Basin Field 146, 147, 149, 151, 159
Osagean strata 190, 193, 194, 203
- brine reflux modelling 30, 209–211
mathematical model 211–214
porosity/permeability changes 214–216
simulation 216–219, 220, 222, 223, 224
- bryozoa, Globigerina Limestone 265
Burnham Formation 286, 288, 290
- Cabo de Gata volcanic province 117–118
- calcite cement 11–12, 13
Cisco Formation 144–146, 148, 157
Osagean strata 190, 193, 194
- calcite dissolution
heterogeneity, and surface characteristics 82
reactions 81–82
and roughness 82, 83–84, 87–93
- calcite spar 82, **83**, 84, 87, 88, 89
- Canyon Formation 142, 143
hydrothermal fluid flow 166–168
paragenetic sequence 144–149, 170
- capillary pressure, drainage 96, 108, 109
- carbon dioxide injection 37
and water–rock interaction 81, 82
- carbon isotopes 12
Miocene carbonate dolomitization 121, 125–129, 131, 132, 133–135
- carbonate platforms
reefal, porosity, XRTM 63–77
transport properties and upscaling 76
- carbonate ramp model, Field X 430, 431
- carbonate reservoirs
characterization 4, 5, 11–13, 22
dolomite, porosity 141
dolomitization 209
fault zones 36, 268–272
flow domains 2, 6
microporosity, network modelling 95–111
- Mississippian chert
hydrothermal fluids 197–200
lithofacies and deposition 183, **184–185**, 186
porosity 179–180
- modelling, and outcrop studies 4, 7, 8, 9
- Pennsylvanian dolomite, porosity 141
- porosity, X-ray CT 61–77
- quality prediction 3, 401–422
Shu'aiba Formation 405, 411–422
Unayzah reservoir porosity 404–405
- seismic attributes 4, 14–15, 17, 334–355
types 6, 234, 236–239
- Castlegate Sandstone, image segmentation 106
- cathode luminescence, dolomite 123–124, 125, 131
- cement *see* calcite cement; dolomite cement
cementation factor 96
cementation modelling 99, 102, 103, 104–106, 111
- chalcedony precipitation 145, 146
Osagean strata 190, 193, 194, 203
- chalk
fracture geometry 281, 283–307
elastic dislocation modelling 291–299
finite-element modelling 299–306
- Chalk Group
seismic velocity change 343
South Arne fault network 331–333, 344–355

- chaos attribute 335, 336, 338, 341, 342–343, 344–345, 347
- chemomechanical processes 12, 312, 323–328
- Cherokee Basin
cherty carbonates 183, **184–185**, 186
geological setting 180–183, *181*
- chert
reservoir porosity
Mississippian 179–180
subaerial v. hydrothermal 200–203
tripolitic 180, **185**, 186, *187*, *189*, 200–201
- Chondrites* 268
- Cisco Formation 142, 143
calcite cementation 144–146, 157
hydrothermal fluid flow 166–168
paragenetic sequence 144–149, 170
- collaboration, multidisciplinary 4, 6–9
- compliance, fractured rock 361
stress-dependence 362–363
- computing *see* interactive visual computing; parallel computing
- COMSOL multiphysics modelling 210, 216–217
- coral, Shu'aiba Formation 408–409
- core analysis, Field X 429–430, 435, *436*
- corrosion-enhanced porosity, Field X 432–444
- Crab Orchard Sandstone 363–367
- crack propagation 13
- Crestal Graben *332*, 334, 352
- Cretaceous, chalk fractures, modelling 281, 283–307
- CT *see* X-ray computed tomography
- Damkohler number *213*, 214
- Danish Central Graben, tectonic inversion 333, 334
- data mining 5, 34
- deformation
comparative studies 3, 283–307
syndepositional 4, 7
- density-driven flow 209–210
mathematical model 211–216
simulation models 216–227
- diagenesis
backstripping 4, 11
and deformation 4, 7
early, Indian Basin Field 155, 157
late, Indian Basin Field *156*, 157–168
Malta 268
middle, and secondary porosity 311
modelling 26, 403–404
overprints, forward seismic modelling 4, 17
regional perspectives, comparative studies 3, 133–135
reservoir typing 6, *234*, 236–239
- dickite 432, 435
- Differential Evolution algorithms (DE-Best DE-Rand) 35, 458, *459*
- diffraction imaging 16
- diffusion models 403
- Digital Image Correlation (DIC) 4, 13
- digital imaging, Pozalagua Quarry 8
- dip *see* seismic dip
- Discontinuous Galerkin method 390–392
- discrete fracture matrix (DFM) modelling 5, 28–29
- discrete fracture network (DFN) modelling 19, 20
- dissolution 11
and dolomitization 11, 125
- flow-through injection experiments 321, 324–326
- hydrothermal origin 157–159, 162–163, 166–168
- Indian Basin Field 146, 147, 149, 161–162, 166
mesodiagenesis 311
Osagean strata *190*, *191*, *192*, 193, 194, 201, 203
- dolomite 3, 11
baroque, Osagean strata *190*, *194*, 195
fluid inclusions 196–197, *198*, 203–204
replacement, Indian Basin Field *145*, 147, 149–151, *154*, *158*, 161
RTM 29–30
- dolomite cement 122–124, 125, 135
Indian Basin Field *145*, 147, 149, 151–153, *154*, *160*, 161, *164*
- dolomite reservoirs 209
porosity 141, 142
Indian Basin Field 144–173
paragenetic sequence 144–149
- dolomitization
Benicassim, NE Spain *31*
density driven flow 210–211
COMSOL multiphysics modelling 210–227
mathematical modelling 211–216
and dissolution 11, 125
freshwater–mesohaline mixing 116, 131–133
Miocene carbonates 116, 117–136
abundance 121–122, 131
C and O isotopes 121, 125–129, 131–135
cement 122–124, 125, 131, 135
CL patterns 123–124, 125, 131
conceptual model 131–133
fluid inclusion analysis 121, 125, *126*, 131, 135
petrography 120, 121–125
replacive 122, *123*, 124, 125, 131, 135
strontium isotopes 121, 129–131, 135
XRD 121, 125
mixing-zone 115–116, 131–133
open and closed systems 210
Osagean strata *190*, *191*, *192*, *194*, 195
- dolostone reservoirs 209
- 'Dorag' dolomite 115, 116
- downdip carbonate facies 142, 169–171
- dynamic modelling 19, 21
- echinoderms, Osagean **184–185**, *186*, *187*
- echinoids, Globigerina Limestone 265
- edge attributes 334, 335, 342, 343, 344–345, 354
- edge-enhancement 335, 336, 342, 343, 344–345
- Ekofisk Formation 332, 333–334, 348, 349, *350*
stress field change 343
- Ekofisk Tight Zone 332, 333, 334
- elastic dislocation modelling 291–299
strike-slip faults
geometry 291–294
mechanical properties 294
stress fields
fault bends 295–297
faulting depth 298
friction on fault 297
kink geometry 297
- elastic moduli, transversely isotropic media 361–362, 372
- electrofacies 232–233

- enhanced oil recovery (EOR) 10, 24, 27
 RTM 36
 'smart water' technique 81
- Estailades Limestone
 network modelling 99, **100**, 106–110, 111
 image segmentation 97–98
- evaporation, Mediterranean 126–128, 129, 131, 134
- fault bends, stress fields 295–297, 299–306
 fault cube 336, 344–346, 347, 350, 352, 353, 355
 fault network mapping, South Arne 331–355
 fault zones
 dynamic behaviour 36
 imaging 13
 Malta 268–269
 architecture 269–272
- Field X
 corrosion-enhanced porosity 432–444
 database 429–430
 diagenesis and reservoir quality 430–433
 geological setting 430, 431
 near-wellbore modelling 436–441
 permeability modelling 428
- finite-difference methods 24
 finite-element modelling, strike-slip faults 299–306
- Flamborough Head chalk
 fracture geometry 285–288, 289, 290
 porosity 283–284
- flow types 6
 flow zone indicators (FZI) **231**, 232–233
 flow-through injection experiments 317–328
 original characterization and dissolution 321
 P-wave velocity 318, 319
- fluid inclusion analysis, Miocene carbonate
 dolomitization 121, 125, 126, 131, 135
- fluid inclusion assemblages
 Indian Basin Field 149–155, 157–159, 162, 171
 Osagean strata 195–197, 198, 199, 200
- fluid-flow processes
 effect of cementation and dissolution 99
 geological impacts **5**, 22–23
 hydrothermal
 Indian Basin Field 166–168
 tectonic valving 167–168
 Osagean strata 197–200, 202, 203
 microporosity 95
 modelling **5**, 20, 21–22
 fractured formations **5**, 25
 multiphase 25, 26–27
 time-lapse studies 359–360
 upscaling **5**, 23
- foraminifera
 Field X 430, 431
 Globigerina Limestone 265–268
 Lower Coralline Limestone 264–265
 Shu'aiba Formation 407, 408
- forward seismic modelling **4**, 17, 403–404,
 411–422
- Fourier transform 335
- fractures 7
 calcite dissolution 81–93
 impact of roughness 89–92
 compliance 361
 stress-dependence 362–363
- Cretaceous chalk
 Flamborough Head 285–288, 289, 290
 mechanical modelling 281, 283–307
 Pegwell Bay 285, 286–287, 288–290
- geometry
 bends 295–297, 299–300, 301–302, 303–306
 concentric rings 285
 corridors 282–283, 285, 286–287, 288–290
 local patterns 283
 regional sets 282, 287, 288
 through-going background 285
 in greater-than-wavelength layer
 thickness 390–398
 grids 28, 29
 Indian Basin Field 144–149, 159, 161, 165
 pygmatic 144, 146, 155, 156
 modelling 19
 fluid flow **5**, 25
 geomechanics **5**, 26, 30, 281–306
 Osagean strata 190, 193, 194
 in sub-wavelength layer thickness 376–390
- freshwater–mesohaline mixing, dolomitization **3**,
 116, 117, 128–129, 130, 131–136
- freshwater–seawater mixing, dolomitization 115–116
- full-azimuth data (FAZ) **4**, 14, 15
- full-waveform inversion (FWI) **4**, 14, 16
- gas *see* hydrocarbons
 gas injection 10, 25, 37
- geological maps 452
- geomechanical modelling **5**, 26, 30, 281–306
- geometric models 403
- geoscience–engineering communication 7
- geothermal reflux model 210, 211
 mathematical model 212–214
 porosity/permeability changes 214–216
 simulation 216–218, 221, 224–226
- Globigerina* 268
- Globigerina Limestone Formation 265–268
 Terminal Hardground 268
- Gnejna Bed 265, 266, 267
- Golden Grove dolomite 116
- Gozo, acoustic velocity and porosity 262–278
 fault zones 268–269
- grainstone
 characterization 314, 316, **317**
 flow-through experiments 319–321
 dissolution 321
- Gravina Calcarenite characterization 314,
 316, **317**
- Great Pearl Bank Barrier 412, 413
- grids
 adaptive 28–29
 geocellular 451, 452
 perpendicular bi-sector (PEBI) 28
 unstructured 27–28
- halite, Mallorca 134
- Heterostegina* 265
- heuristic modelling 403
- history matching **5**, 33–34
- Hope Gate Formation dolomite 115, 116
- Huapache Fault 142, 144
- hydraulic-process models 403

- hydrocarbons
 - Indian Basin Field
 - fluid inclusions 153, 155, 162–163
 - migration 145, 149, 153, 159, 165, 167
 - reservoir properties 169–171
 - microseeps 454
- hydrofracturing 159, 161
- hydrohalite, Indian Basin Field 152, 153
- hydrothermal fluids
 - Arkoma Basin 197, 199–200
 - Indian Basin Field 157–159, 162–163, 170–171
 - composition 159
 - downdip strata 142, 169–171
 - fluid flow 166–168
 - migration, MVT ores 183, 197
 - Osagean strata 197–201, 202, 204
 - reservoir porosity 141
- hysteresis 25
- Idd el Shargi North Dome, seismic anisotropy 16
- Il Mara Member 264, 265, 266, 267, 268
- Il-Maghlaq Fault 268
- image segmentation, pore space 96, 97–98
- imbibition and drainage 100–101, 104–105, 106, 107, 110, 111
- Indian Basin Field
 - deformation 159, 161
 - diagenesis 155, 156, 157–168
 - hydrothermal origin 157–159, 162–163
 - diagenetic and stratigraphic model 168–173
 - dissolution 161–162
 - dolomite
 - paragenetic sequence 144–149
 - sampling 144
 - fluid inclusion assemblages 149–155, 162, 171
 - anhydrite 155, 165
 - dolomite cement 151–153, 160, 161–162, 164
 - entrapment 151–153, 155, 157–159, 162, 164
 - hydrocarbons 153, 155, 162–163, 165–166, 167
 - replacement dolomite 149–151, 158, 160
 - salinity 151, 152, 153
 - formation 172
 - geological background 142–144
 - hydrothermal fluids 157–159, 162–163
 - composition 159
 - downdip strata 142, 169–171
 - fluid flow 166–168, 170–171
 - meteoric water 163, 165, 166
 - oxygen and strontium isotope data 155, 166–167, 169, 170
 - replacement dolomite 145, 147, 149–151, 154, 158, 161
 - tectonic valving 167–168, 171
- industry applications, global context 2–6
- interactive visual computing 447–463
 - data visualization and analytics 449–450
 - hydrocarbon microseep and reservoir data 454
 - post-processing 454–457
 - reservoir flow simulator steering frameworks 461–463
 - reservoir modelling 450–453
 - SRV reconstruction 453–454
 - technology-driven 448
 - user-driven 448–449
 - visual data interaction 450
 - visual data modelling 449
 - visualization high dimensional data 457–461
- invasion percolation algorithm 100–101, 111
- karst features 16
 - Llucmajor reef-rimmed platform 72
 - Osagean strata 190, 193, 200, 203, 204
 - Shu'aiba Formation 420, 421
- Khuff Formation, seismic attributes 15
- kink geometry 297–298
- kriging 19, 401
- Kulindrichnus* 266
- La Molata Miocene carbonates 3, 117, 118–119
 - dolomitization 121–125, 122, 131–136
 - palaeoclimate 119
 - palaeotopography 119, 120
- Lago Mare facies 119
- Laramide Orogeny 142, 144, 158, 161, 165, 168, 172
- late-burial corrosion 427, 432, 433
 - see also* corrosion-enhanced porosity
- layering, and seismic waves 376
 - sub-wavelength thickness 376–390
- Lepidocyclus* 265
- LiDAR outcrop images 9, 29
 - Amellago, Morocco 8
- Llucmajor reef-rimmed platform 63
 - porosity variability 72–73
- Lower Coralline Limestone Formation 264–265, 266, 267
- macronetwork, pore-throat network 98, 99, 111
- Mallorca, Miocene dolomitization 133–136
 - see also* Ses Sitjoles boreholes
- Malta
 - acoustic velocity and porosity 262–278
 - fault zones 268–269
 - architecture 269–272
 - Oligo-Miocene sedimentology 264–268
 - Oligo-Miocene tectonics 268
 - pre-faulting diagenesis 268
- Marathon-Ouachita Orogeny 142, 144, 161, 182
- marble, calcite dissolution experiments 82, 83, 84, 85–87, 88, 89, 90, 92
- Mediterranean Sea
 - evaporation 126–128, 129, 134
 - Western, dolomitization 133–136
- megaquartz precipitation
 - Osagean strata 190, 193–194
 - fluid inclusions 195–196, 197, 198, 203–204
- Meramecian, stratigraphy 182
- Mercury Injection Capillary Pressure (MICP) 13
- Messinian Salinity Crisis 119
- meteoric water, Indian Basin Field 163, 165, 166
- Mgar ix Xini Bed 265, 266, 267
- micritization, Osagean strata 190, 191
- microflora and fauna, Shu'aiba Formation 407–409
- microfractures 160, 161, 165
- micronetwork, microporosity 98, 99, 104, 107
- microporosity 62, 70, 75–76
 - and acoustic velocity 262
 - multiscale network modelling 95–111
 - Bentheimer Sandstone 98, 101–103, 104–106
 - construction 98–100
 - Estailades Limestone 97–98, 99, 100, 106–110

- mineral reactions, in fractures 81
- Miocene carbonates, SE Spain 117, 118
 - dolomitization 116, 117–136
 - carbon and oxygen isotopes 121, 125–129
 - conceptual model 131–133
 - and dissolution 125
 - fluid inclusion analysis 121, 125, 126, 135
 - petrography 120, 121–125
 - strontium isotopes 121, 129–131, 135
 - XRD 121, 125
 - palaeoclimate 119
 - palaeotopography 119, 120
 - sequence stratigraphy 118–119
- Mississippi Valley Type Pb–Zn deposits 183, 197
- Mississippian
 - carbonate reservoir
 - chert porosity 179–180
 - subaerial v. hydrothermal 200–203
 - sea-level change 182–183
- Mississippian-Pennsylvanian unconformity 200–201, 204
- mixing-zone dolomitization 115–116
 - freshwater–mesohaline, Miocene carbonates 116, 117, 128–129, 131–136
- modelling tools 5, 24–33
- monitoring, real time 5, 33–38
- Mont Sant' Angelo Formation
 - flow-through injection
 - permeability and velocity 322
 - and porosity 320, 321, 323
 - mudstone characterization 312, 313, 314, 316, 317
- Monte Acuto Formation
 - flow-through injection
 - permeability and velocity 322
 - and porosity 318, 319–320, 321, 326
 - mudstone characterization 314, 316, 317
- mudstone
 - characterization 312, 313, 314, 316, 317
 - flow-through experiments 320, 321
 - dissolution 321, 326–327
- multipoint statistics 402
- multiscale integration and proxies 5, 18–23
- multitouch displays 30, 32

- nannofossils, calcareous 407
- Naxos marble 83
 - flow-through experiment 85, 89, 90
- near-wellbore modelling, Field X 435, 436–441
- Neighbourhood Algorithm 35, 458, 459
- network models, microporosity 96–111
 - characterization and complexity 99–100
 - grain-based approach 98, 99
 - imbibition and drainage 100–101, 104–105, 106, 107, 110, 111
 - pore space 96, 98
 - tiled image approach 98–99
- Newhaven Chalk Member 285
- Nijar, Miocene dolomitization 133–136
- novel experiments 4, 13–14
- Nuclear Magnetic Resonance (NMR) 4, 13

- off-diagonal complexity 99–100, 103, 104, 108, 110–111
- Oligo-Miocene sedimentology, Malta 264–268
- oolite, calcite dissolution experiments 82, 83, 84, 85, 87, 88, 89
- Ophiomorpha nodosa* 265, 267
- Osagean strata
 - chert porosity 200–203, 204
 - entrapment temperature 197, 198, 199, 200, 203
 - fluid inclusion assemblages 195–197, 198, 199, 200
 - genetic stratigraphy 186–190
 - hydrothermal system 197–200, 202
 - lithofacies and deposition 183, 184–185, 186
 - palaeogeography 182, 183
 - paragenetic sequence 190–195
 - stratigraphy 182
 - transgressive-regressive cycles 186–190
- Ouachita Fold Belt 180, 181
- outcrop studies 36
 - and reservoir modelling 4, 7, 8, 9, 451–452
- oxygen isotopes 12
 - Indian Basin dolomites 155, 159, 166–167, 169
 - Miocene carbonate dolomitization 121, 125–129, 131, 132, 133–135

- P-waves
 - acoustic wavefront imaging 376, 377
 - effect of rock layering 376
 - velocity
 - porosity prediction 262–263, 272–278
 - porosity variation 312, 313, 317, 318
 - flow-through injection 318, 319–320
 - stress-dependent anisotropy 364–370
 - wave-guiding 377–390
- packstone
 - characterization 315, 316, 317
 - and dissolution 321, 325–326
- Osagean
 - oid 185, 186
 - sponge-spicule 184, 186, 188
- Paleophycus* 268
- paragenesis, sequence stratigraphy
 - Indian Basin Field 144–149, 170
 - Osagean strata 190–195
- parallel computing 28, 34
- Particle Swarm Optimization (PSO) algorithm 35, 458, 459
- Peclet number 212, 213, 214
- Pegwell Bay chalk, fractures 285, 286–287, 288–290
 - porosity 283–284
- permeability 10, 62
 - density-driven flow
 - mathematical model 214, 215–216
 - simulation model 216, 222, 223, 225–226
- Estailades Limestone 108, 110
- flow-through injections 317–319
- index multipliers 428
- Klinkenberg-corrected 312, 313, 318
- modelling, late-burial corrosion 428, 433–444
- reflux dolomitization model 219
- and roughness 92
- sandstone cementation study 104–105, 106
- Ses Sitjoles boreholes 64, 69
- X-ray CT 11
- Peschici Formation
 - flow-through experiments
 - dissolution 321, 324–325
 - permeability and velocity 322
 - mudstone characterization 314, 315, 316, 317

- petrography, Miocene carbonates
dolomitization 120, 121–125
- petroleum *see* hydrocarbons
- Planolites* 268
- polymer flooding 10
- pore stiffness 315–317
dissolution and stress coupling 322–323, 324, 326
- pore typing 230, **231**, 232, 239–240
and acoustic velocity 262
- pore-network experiments, flow-through injection
317–328
- pore-network modelling 11–12, 27, 62
microporosity 96–111
- pore-scale simulation **5**, 11, 21, 26–27, 62
microporosity 95, 96
- pore-space characterization 95–96, 312
- pore-space compressibility 312
- pore-throat networks 96, 97–98, *102*, *103*, 104
- porosity 9–10
chert, Mississippian reservoirs 179–180, 190
subaerial v. hydrothermal 200–203
corrosion-enhanced 433–444
density-driven flow
mathematical model 214–216
simulation models 216, 222, 223, 224, 225–226
dolomite reservoirs 141
flow-through injections 317–328
intragranular 96
and mesodiagenesis 311
mouldic 74–75, 125, **184–185**, *192*, 238, 268
North Sea chalk 283–284
prediction 404–405
secondary 311–312
Ses Sitjoles boreholes 64–77
estimation and effect of resolution 73–76
spatial variability 72–73, 74
vuggy 82, 95, *156*, 248, 249
X-ray CT 11, 61–77
- porosity-permeability relationship 11, 62, 69
- porosity-velocity relationship
Malta outcrop studies 13, 262–264, 272–278
effect of fault displacement 276, 277
effect of fault zone architecture 272, 275, 277
effect of sedimentary facies 272, 273
- post-processing 454–457
- Pozalagua Quarry, digital imaging 8
- pressure solution, grain-to-grain *190*, *192*, 193
- Pricaspian Basin, seismic attributes *15*
- ptygmatic fractures 144, *146*, 155, *156*
- pyrite precipitation *190*, 194, 197
- Ras Ir Raheb Bed 266, 267, 268
fault zone architecture 269, 270, 271
- reactive transport modelling (RTM) **3**, **5**, 10, 22, 24,
25–26, 29–30
dolomitization 210
production timescales 36
- replacement dolomite
Indian Basin *145*, 147, 149–151, *154*, *158*, 161
Miocene carbonates 122, *123*, 124, 125, 135
- representative elementary volume (REV) 21
- Reqqa Bed 265–266, 267
- reservoirs *see* carbonate reservoirs
- rhodoliths, Lower Coralline Limestone 264
- rock physics **4**, 12–13, 323–328
- rock-typing **4**, 10, 11, 22, 229–255, 261
depositional (DRT) 230, **231**, 234–236
dynamic **231**, 233
integrated **231**, 232
partitioning **231**, 232–233
petrophysical (PRT) 229–255
workflow 233–244
data scenario 233–234, 246, 252
definition 234, 240–241, 248–249, 253, 255
determination 234, 241, 242, 249–250, 255
DRT 234–236, 246–247, 252–253, 254
dynamic validation 241–242, *243*, 250, 255
pore typing 230, **231**, 232, 239–240, 248, 253
realization 234, 242, 244, 250–251, 255
reservoir typing 234, 236–239, 247–248, 253
Tengiz Field 246–251
- Rodaliquilar caldera 119, *120*
- roughness
impact on calcite dissolution 82, 83–84, **87**, 89–92
scale dependence 91–92
see also asperity
- rudists, Shu'aiba Formation 407–408, 411, 412, *413*
- S-wave velocity
and flow-through injections 317, 318
porosity prediction 262–263, 272–278
stress-dependent anisotropy 364–367
reservoir model 367–370, *371*
- salinity, Indian Basin Field 151, 152, 153
- saturation component 96
- scaling relationships **5**, 23
- Schizaster* 265, 266, 267, 268
- Scutella* 265, 266
- sea-level change
Mississippian 182–183
Osagean 187–190
post-TCC 131–132, 134
- seawater, dolomitization 116, 131, 132–133
- sedimentation, and deformation **4**, 7
- SedSim stratigraphic forward modelling 403–404
Shu'aiba Formation 411–422
- seismic acquisition and processing 16
- seismic amplitude variation 334, 335, 341–342, *347*,
352, *354*
- seismic attributes **4**, 14–15, 17, 334–355
- seismic dip
causality 337, 340
change 334, 335
consistency 337–338, 340, 343
continuity 338, 340
estimation 335–338
globally consistent 339–341, 345, 354
reciprocity 336–337, 340
surface reconstruction 338
time-lapse seismic analysis **5**, 343, 350–351, 355
uncertainty 334
XYZ v. IJK space 339, *340*, *342*, 352
- seismic imaging 16
- 'seismic triple-combo' workflow 17, 334–335, 336
- seismic velocity, anisotropy **4**, 16, 17–18, 359–360
stress-dependence 360–372
reservoir model 367–370
see also acoustic velocity; wave guiding

- Ses Sitjoles boreholes 63–64
 permeability 64, 69
 porosity 64–77
 estimation and effect of resolution 73–76
 macroplugs 64, 65, 69–70, 76
 microplugs 64, 65–69, 70–72, 73–74, 75
 miniplugs 64, 65–69, 70, 73, 74, 75
 spatial variability 72–73, 74
 XRCT 65–77
 XRMT 65–69
- shale
 Pennsylvanian **185**, 186, 188, 190, 191
 Osagean strata 190, 193
- Shaybah Field 409, 410, 411, 413
- Shu'aiba Formation
 age 405–407, 411
 biocomponents 407–409, 411–413, 414, 418–421
 compaction 416
 diagenesis 416–417, 420, 421
 geology 405–411
 microflora and fauna 407–409
 stratigraphic forward modelling 405, 411–422
 stratigraphy 406, 409–411, 413, 415
 tectonic subsidence 416
- silicification, Osagean strata 190, 191, 192, 201, 203
- sketch-based interface modelling (SBIM) **5**, 32, 33
- Solnhofen limestone
 calcite dissolution experiments 82, **83**, 84
 flow-through experiment 85–89, 90, 92
- South Arne Field 332–333
 fault network 331–332, 334
 4D seismic analysis 350–351
 components 346–351
 ENE–WSW trend 349–350, 352–353, 355
 north-south trend 349
 WNW–ESE trend 348, 349, 350
 controls on fluid distribution 351–353
- Spain, Upper Miocene carbonates 116, 117, 118
- sponge-spicules, Osagean **184–185**, 186, 188, 201, 203
- spontaneous potential (SP) **5**, 37–38
- static modelling 19
- steam injection 10
- stimulated reservoir volume reconstruction 453–454
- Stokes equation 62
- Stone I and II models 25
- strain accommodation 13
- stratigraphic forward modelling 403–404
 Shu'aiba Formation reservoir quality 411–422
 Unayzah reservoir porosity 404–405
- strontium isotopes
 Indian Basin Field dolomites 155, 166–167, 169
 Miocene carbonate dolomitization 121, 129–131, 132, 135
- stylolites 13, 26, 145, 147, 150, 159, 161, 375
 Ekofisk Formation 333–334
 Field X 430, 432, 433, 435
 Osagean strata 190, 191, 193
- subaerial exposure, and porosity 200–201, 203, 204
- subsurface imaging **4**, 14–18
- surfactant injection 10
- tectonic valving 167–168, 171
- Tengiz Field 244–246
 porosity-permeability 237, 239
 rock typing workflow 237, 243, 245, 246–251
- Terminal Carbonate Complex 119, 131, 134
 unconformity 124–125
- Thalassinoides* 265, 266, 268
- Thanet Anticline 285
- time shifts 343, 345, 346
- time-lapse studies **4**, 36–38, 343, 350–351, 355
 fluid flow 359–360
 and stress variation 360
- Tomographic Fracture Imaging (TFI) **5**, 37, 38
- Tor Formation 332, 333–334, 348, 350
- transgressive-regressive cycles 186–190
- TripleComboEdge 342
- Unayzah reservoir, porosity prediction 404–405
- Upper Chalk Formation 285
- upscaling, fluid-flow processes **5**, 21, 22, 23
- variogram-based techniques 401–402
- visualization and interaction **5**, 30, 32, 34–35, 447–463
- vugs, Indian Basin Field 152, 156, 161
see also porosity, vuggy
- wackestone, argillaceous, Osagean **184**, 186, 187, 188–189, 190
- Wafra First Eocene Field 245, 251–252
 rock typing workflow 252–255
- warping, 3D 346, 353, 354
- water flooding
 controlled salinity 10, 25
 spontaneous potential **5**, 37–38
- water–rock interactions 81
 carbonate reservoirs 82–93
 Indian Basin Field 166
- wave cut platforms 285, 286, 289
- wave guiding 376, 377–390, 392–399
- weathering *see* subaerial exposure
- Welton Formation 286, 287, 290
- wettability alteration 10, 13
- wide-azimuth data (WAZ) **4**, 16
- Wisconsin Arch dolomite 115, 116
- X-ray computed tomography (CT)
 high-resolution **4**, 10–11, 12
 multi-resolution, carbonate porosity 61–77
- X-ray micro-tomography (XRMT) 62, 96
 microporosity modelling 96–111
 image analysis 97–98
 network modelling 100–104
 two-scale network construction 98–100
- Ses Sitjoles boreholes 65–69
- X-ray powder diffraction (XRD) 121, 125
- Xlendi Member 265, 267
- Zebra fabrics 145, 146, 147, 157

Fundamental Controls on Fluid Flow in Carbonates

Current Workflows to Emerging Technologies

Edited by

S. M. Agar and S. Geiger

This volume highlights key challenges for fluid-flow prediction in carbonate reservoirs, the approaches currently employed to address these challenges and developments in

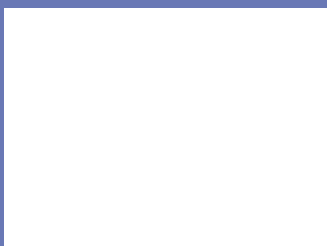


fundamental science and technology. The papers span methods and case studies that highlight workflows and emerging technologies in the fields of geology, geophysics, petrophysics, reservoir modelling and computer science. Topics include: detailed pore-scale studies that explore fundamental processes and applications of imaging and flow modelling at the pore scale; case studies of diagenetic processes with complementary perspectives from reactive transport modelling; novel methods for rock typing; petrophysical studies that investigate the impact

of diagenesis and fault-rock properties on acoustic signatures; mechanical modelling and seismic imaging of faults in carbonate rocks; modelling geological influences on seismic anisotropy; novel approaches to geological modelling; methods to represent key geological details in reservoir simulations and advances in computer visualization, analytics and interactions for geoscience and engineering.

Visit our online bookshop: <http://www.geolsoc.org.uk/bookshop>

Geological Society web site: <http://www.geolsoc.org.uk>



Cover illustration:

Multi-touch operations applied to post-processing of a reservoir model. The user is pulling the model apart into several arbitrary blocks to view properties inside the model.

Photo by M. Costa Sousa.